










Absolute frequency referencing in the long wave infrared using a quantum cascade laser frequency comb

K. N. KOMAGATA,^{1,*}  M. GIANELLA,²  P. JOUY,³
F. KAPSALIDIS,⁴  M. SHAHMOHAMMADI,⁴
M. BECK,⁴ R. MATTHEY,¹  V. J. WITTEW, ¹  A. HUGI,³
J. FAIST,⁴  L. EMMENEGGER,²  T. SÜDMEYER,¹ 
AND S. SCHILT¹ 

¹Laboratoire Temps-Fréquence, Institut de Physique, Université de Neuchâtel, Avenue de Bellevaux 51, 2000 Neuchâtel, Switzerland

²Empa, Laboratory for Air Pollution / Environmental Technology, 8600 Dübendorf, Switzerland

³IRsweep AG, Laubisrütistrasse 44, 8712 Stäfa, Switzerland

⁴Institute for Quantum Electronics, ETH Zurich, 8093 Zurich, Switzerland

*kenichi.komagata@unine.ch

Abstract: Optical frequency combs (OFCs) based on quantum cascade lasers (QCLs) have transformed mid-infrared spectroscopy. However, QCL-OFCs have not yet been exploited to provide a broadband absolute frequency reference. We demonstrate this possibility by performing comb-calibrated spectroscopy at $7.7\ \mu\text{m}$ ($1305\ \text{cm}^{-1}$) using a QCL-OFC referenced to a molecular transition. We obtain $1.5 \cdot 10^{-10}$ relative frequency stability (100-s integration time) and $3 \cdot 10^{-9}$ relative frequency accuracy, comparable with state-of-the-art solutions relying on nonlinear frequency conversion. We show that QCL-OFCs can be locked with sub-Hz-level stability to a reference for hours, thus promising their use as metrological tools for the mid-infrared.

© 2022 Optica Publishing Group under the terms of the [Optica Open Access Publishing Agreement](#)

1. Introduction

The enticing prospect of highly sensitive and selective molecular detection has spurred the development of mid-infrared (MIR) spectrometers [1,2], having strong implications for example in the fields of security [3], health [4], food production [5], and others [6–8]. While Fourier transform infrared spectrometers (FTIRs) based on thermal sources have, for several decades, been the working horse for MIR spectroscopy, optical frequency combs (OFCs) [9] have emerged in the last two decades as the new tool for spectroscopy [1]. In particular, they have allowed the measurement of transition frequencies with unprecedented accuracy [10]. Indeed, they can provide a broadband ruler for measuring optical frequencies through referencing to only two frequencies. Moreover, they are polyvalent in their application to spectroscopy [11], e.g. in dual comb arrangements [12–16], combined with an FTIR [17,18], or in open or closed loop comb-assisted schemes [19–21].

So far, nonlinear frequency conversion has been the main way to perform MIR spectroscopy with referenced OFCs generated in the near-infrared (NIR), at the cost of added complexity, reduced optical output power, and the necessity of sufficient seed power. Integrated photonics based on lithium niobate or silicon nitride promise small-footprint conversion with low pulse energy, but only to wavelengths up to $4.5\ \mu\text{m}$ [8,14,22–24]. In the long-wave infrared ($8\ \mu\text{m}$ to $12\ \mu\text{m}$) and beyond, several experiments successfully determined the absolute frequency of molecular transitions by performing nonlinear frequency conversion [25–35]. The obtained accuracies were typically in the 100-kHz range in the Doppler-limited regime and down to 22 Hz in the Doppler-free regime [10].

In 2012, quantum cascade lasers (QCL) demonstrated a breakthrough by allowing the direct generation of OFCs in the MIR [36,37]. Since then, the development of a commercial dual comb spectrometer based on QCLs has had a disruptive impact in the fields of chemistry and biology [38,39]. The success of QCLs can be attributed to their small footprint and simple operation. Furthermore, they can be conveniently controlled with their temperature [40], driving current [41–43], and through radio-frequency (RF) injection locking, which locks their GHz-level repetition rate [44–46]. The mode locking of their optical mode is based on four-wave mixing, and while not leading to pulse formation, results in equidistant teeth which were tested to the $7.5 \cdot 10^{-16}$ level [40]. Their phase coherence [42,47], sub-kHz linewidth [41], and sub-Hz locking stabilities [43] promise that QCL-OFCs can be used for metrological purposes. As a matter of fact, QCL-OFCs emitting in the THz range have already been fully referenced and used for spectroscopy [48,49].

However, a fully referenced MIR QCL-OFC has not yet been demonstrated. As has been done for THz QCLs [48], the repetition rate can be locked by RF injection locking and the offset frequency can be controlled via the driving current of the QCL [41,43,50]. Self-referencing via f-to-2f interferometry [51] is not currently achievable for QCLs, although progress in generating picosecond and femtosecond pulses has recently been demonstrated [52,53]. Instead, the QCL-OFC can be locked to a high accuracy MIR frequency reference [54]. These can be obtained by locking MIR lasers to sub-Doppler molecular transitions [55–59] with frequency stabilities and accuracies as good as 0.1 Hz [56] and 90 Hz [58], respectively. Through this approach, we can conceive a QCL-OFC with Hz-level stability and accuracy in a fully MIR implementation.

In this work, we demonstrate for the first time to the best of our knowledge a fully referenced MIR QCL-OFC. We characterize its frequency stability and accuracy and use the broadband reference to perform comb-calibrated Doppler-limited spectroscopy with accuracies on par with state-of-the-art solutions relying on nonlinear frequency conversion [29,35].

2. QCL-OFC referenced to a molecular transition

We have implemented the frequency-referenced QCL-OFC according to the setup detailed in Fig. 1(a). We have locked a distributed-feedback (DFB) QCL (Alpes Lasers) labelled DFB-QCL1 to the R(8) molecular transition in the ν_1 fundamental band of N_2O at about 1292.3 cm^{-1} using wavelength modulation spectroscopy (WMS). A laser driver and temperature controller developed at the University of Neuchâtel was used to drive the QCL at an average current of 436 mA and to stabilize it at a temperature of 23°C . A fast modulation at a frequency f_{wms} of about 50 MHz was applied to the laser current via a dedicated bias-tee, which was custom made as most commercially-available bias-tees have a low-frequency cut-off of around 100 kHz that slightly limits the actuation bandwidth of the QCL. The RF power at the bias-tee input was around -10 dBm . The modulation index is roughly estimated to be between 0.25 and 0.5 from Fig. 1(e). After passing through a gas cell (Wavelength Reference, as all gas cells mentioned in this paper) with a length of 1 cm filled with 10% N_2O at 5 mbar pressure, the beam was detected using a photodetector (PVM1-4TE-8/MIPDCv2-F-250, Vigo System). The low concentration of N_2O was due to contamination by water vapor (see Section 4). The DC and AC components of the detector output signal were split using another bias-tee. All RF components used in this work, unless specified, are off-the-shelf commercial devices from Mini-Circuits. All electronic oscillators used were referenced to a GPS-disciplined hydrogen maser to ensure their long-term stability and accuracy.

The detector DC signal provided the optical transmission through the gas cell [see Fig. 1(b)]. The AC signal was filtered, amplified, and demodulated using an analog mixer at the modulation frequency f_{wms} , providing a WMS derivative signal featuring a slope of about 25 mV/MHz and a zero-crossing point near the center of the transition [see Fig. 1(c)]. The linear range is about 16 MHz. We note that residual amplitude modulation generated a voltage offset, breaking

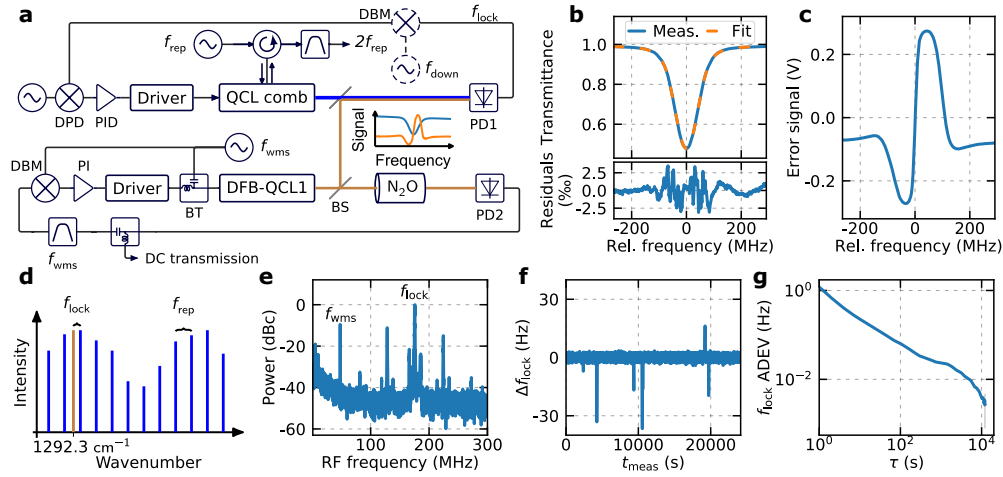


Fig. 1. QCL-OFC stabilization to a molecular reference. (a) Schematized experimental setup. One comb line of the QCL comb is locked to a molecular transition using a DFB-QCL. The intermode beat frequency is locked by RF injection locking. DPD: digital phase detector, PD: photodetector, BS: beam splitter, DBM: double balanced mixer, BT: bias-tee. (b) DC transmission of PD2 when the frequency of DFB-QCL1 is scanned across the N_2O R(8) molecular transition (~ 38.742 THz) and fit with a Voigt profile. The residuals are shown in the lower panel. (c) Error signal obtained by demodulating the high-pass filtered signal of PD2, giving a zero-crossing point with a slope of 25 mV/MHz near the center of the transition. (d) Schematized equidistant spectrum of the QCL comb (blue) and DFB-QCL1 (brown), illustrating the transfer of the frequency reference given by the latter. (e) Spectrum of the signal from PD1 (20 kHz resolution bandwidth), showing f_{wms} , the beat between DFB-QCL1 and the QCL comb, and its sidebands. (f) Hz-level frequency fluctuations of f_{lock} during a measurement of 6 hours. (g) Corresponding Allan deviation (ADEV) of f_{lock} showing sub-Hz stability beyond integration times (τ) of a few seconds.

the symmetry of the error signal. The error signal was fed to a proportional-integrator (PI) servo-controller (model LB1005-S, New Focus) to generate a feedback signal, which acted on the QCL driving current via the laser driver to stabilize the emission frequency to the zero-crossing point of the error signal. We recorded the error signal from the error monitor channel of the servo controller, which induced saturation to the signal at ± 330 mV [see Fig. 1(c)]. This did not affect the locking-point around zero voltage.

The QCL-comb chip was designed and fabricated at ETH Zurich. A wire bond connects the laser active area to a dedicated (RF) port on a printed-circuit board (PCB) designed by IRsweep AG, which allows for efficient RF injection and extraction of the intermode beat signal. The comb was operated at an average current of 1150 mA and a temperature of 16°C using a current and temperature controller developed and fabricated at University of Neuchâtel. The intermode beat frequency at 9.75 GHz was stabilized by RF injection-locking [46] using 20 dBm of RF power injected in the laser chip. A circulator (SFC0712, Fairview Microwave) was used to simultaneously inject the master signal and extract the second harmonic of the intermode beat, which allows monitoring the successful injection locking (monitoring at the intermode beat frequency was not possible due to the weakness of the extracted signal with respect to the strong injected RF signal and the limited isolation of the circulator).

Part of the DFB-QCL1 beam was split by a beam-splitter (BSW510, Thorlabs) before the gas cell to be heterodyned with the QCL-OFC on a fast photodetector (UHSM-10.6 PV-4TE-10.6-0.05-butt, Vigo System). The beams were focused on the photodetector with a lens (2-inch

focal length). The heterodyne beat between the comb and DFB-QCL1 was detected beyond the 1.2-GHz bandwidth (specified by the manufacturer) of the photodetector. The heterodyne beat [see Fig. 1(e)] was amplified and compared in phase with a reference signal in a 200-MHz bandwidth digital phase detector (DXD200, MenloSystems) to generate a phase error signal. After amplification in a P-I²-D servo-controller (D2-125, Vescent Photonics), the resulting correction signal was applied to a modulation port of the laser driver to correct the QCL-OFC current. When necessary, the heterodyne beat was frequency-down-mixed with an RF signal f_{down} to fit the 200-MHz bandwidth of the phase detector. The signal-to-noise ratio (SNR) of the frequency-shifted signal was sufficient to obtain phase locks with beat notes of up to 1.5-GHz offset frequency.

Closing the loop, the heterodyne beat is locked at frequency f_{lock} and features Hz-level fluctuations [Fig. 1(f)], with a stability of 2 Hz and ~ 10 mHz at 1-s and 10^4 -s integration times, respectively [Fig. 1(g)]. We note moreover that both the phase lock and the RF injection locking can be maintained during more than 6 hours. Minimization of back-reflections to the QCL-OFC was key to achieve a stable phase-lock. This was realized by attenuating the beam by 95% right after its collimation [60].

In this way, one comb line of the QCL-OFC is referenced to a molecular transition while the lock of the mode spacing allows determining the optical frequency of each comb line with the accuracy of the molecular reference. Thus, the comb acts as an optical frequency reference over its entire emission bandwidth [15-dB bandwidth of 40 cm^{-1} , see Fig. 2(e)] with comb lines spaced by $f_{\text{rep}} = 9.75 \text{ GHz}$ as schematized in Fig. 1(d). The center frequency of the N_2O R(8) transition is known within 72 kHz [29], however, the offset Δf between the locking point of DFB-QCL1 and the transition center (including the pressure shift) needs to be determined. To this end, DFB-QCL1 was scanned across the transition while recording the error signal and the

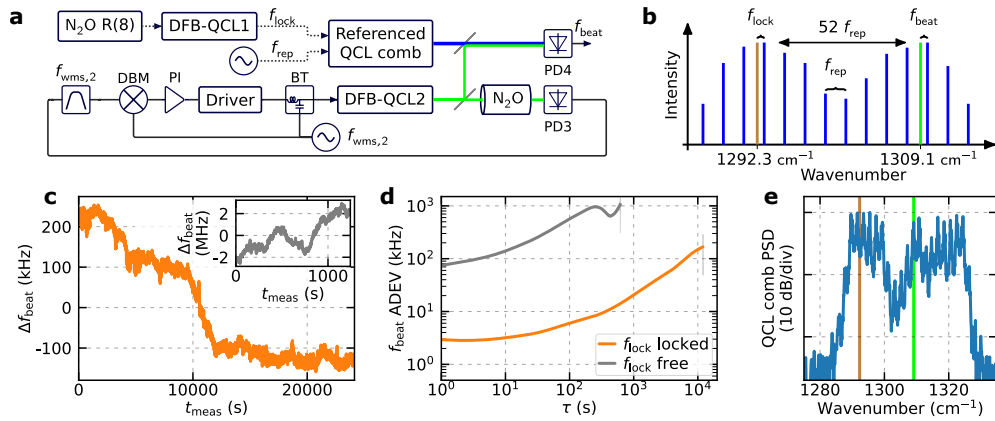


Fig. 2. Assessment of the frequency stability of the stabilized QCL-OFC. (a) Setup comprising the stabilized comb that is controlled by the two frequencies f_{lock} and f_{rep} . f_{lock} determines the offset between the stabilized DFB-QCL1 and one comb line. DFB-QCL2 is locked to a molecular transition in the same way as DFB-QCL1. (b) Schematized spectrum representing the QCL-OFC, DFB-QCL1, and DFB-QCL2 in blue, brown, and green, respectively. The beat note between the comb and DFB-QCL2 is denoted f_{beat} . (c) Frequency fluctuations of f_{beat} when f_{lock} and f_{rep} are stabilized according to section 2. The inset shows a measurement in the absence of f_{lock} stabilization. (d) Corresponding Allan deviation (ADEV) of f_{beat} with open and closed loop of f_{lock} . (e) QCL comb power spectral density (PSD) measured with an FTIR. The emission frequencies of the DFB-QCLs are indicated with vertical lines according to colors from (b).

DC transmission with an oscilloscope (PicoScope 5444D, Pico Technology) prior to locking. A relative frequency scale was obtained from the beat note with one comb line in an open loop [19]. We retrieved Δf from the offset between the zero-crossing point of the error signal and the line center, obtained through fitting of the DC transmission with a Voigt profile [see Fig. 1(b,c)]. The absolute frequency of the locking point was then computed from the center frequency of the transition [29], the offset Δf , and the pressure shift. The frequency stability and accuracy of the referenced QCL-OFC are assessed in sections 3 and 4, respectively.

3. Frequency stability of the stabilized QCL-OFC

We assessed the frequency stability of the stabilized QCL-OFC by locking a second DFB-QCL, named DFB-QCL2, in the same manner as DFB-QCL1, using WMS [see Fig. 2(a)]. DFB-QCL2 was operated at a current of 199 mA and at a temperature of 7°C, so as to probe the R(30) transition of the ν_1 fundamental band of N₂O in a second gas cell of 1-cm length filled with 50% N₂O at a pressure of 1.5 mbar. The beam transmitted through the cell was detected on a photodetector (LabM-I-10.6, Vigo System), labeled PD3. Part of the beam was combined with the comb and focused on a fast photodiode (UHSM-10.6 PV-4TE-10.6-0.05-butt, Vigo System), labeled PD4, using a lens (1-inch focal length). This beat signal provides an out-of-loop measurement to assess an upper bound of the comb frequency stability.

Indeed, while similar components were used, both DFB-QCLs were locked to different gas cells and at different wavelengths [Fig. 2(b)], such that their frequency fluctuations can be considered as fully uncorrelated. Hence, an upper limit to the frequency instability of the QCL-OFC can be assessed from the beat signal f_{beat} between DFB-QCL2 and one of the comb lines. This measurement is shown in Fig. 2(c,d), where the frequency fluctuations and the Allan deviation of the beat frequency f_{beat} are shown.

The peak-to-peak frequency fluctuations are on the order of 300 kHz over a period of 6 hours. A 3-kHz frequency instability is obtained at 1-s integration time while it increases to 6 kHz at 100 s and 57 kHz at an hour. As expected, fluctuations of f_{beat} increased significantly when f_{lock} was open. The frequency instability at 1-s integration time for the comb with only RF injection locking is 74 kHz and it increases to 570 kHz at 100-s integration time [Fig. 2(c,d)].

Back-reflections to the DFB-QCLs were found to distort the error signal (etalon fringes). Therefore, these were minimized, e.g., the active regions of the fast photodiodes were moved outside of the focal points of the beams. Nevertheless, these are still believed to be the main source of drift of the laser frequencies.

4. Absolute frequency accuracy and spectroscopic measurement

In section 3, we assessed the frequency stability of the stabilized comb. In this section, we assess the absolute frequency accuracy by referencing DFB-QCL2 to the comb, scanning it over different molecular transitions, and comparing the obtained frequencies with experimental values reported in literature with 100 kHz-level accuracies. Then, we also used our setup to measure a less accurately-known transition.

The setup is shown in Fig. 3(a). The frequency comb was stabilized as in Fig. 1(a). DFB-QCL2 (in this section, $f_{\text{wms},2}$ was turned off) was heterodyned with the stabilized comb on PD4. Their beat signal at frequency f_{beat} was mixed with a frequency f_{sweep} , and the mixing product was compared in phase with a reference frequency $f_{\text{lock},2}$ in a digital phase detector (DXD200, Menlo Systems). The resulting phase error signal was used to phase-lock the DFB to the comb, with a tunable frequency offset by sweeping f_{sweep} , which is generated by a digital lock-in amplifier (UHFLI, Zurich Instruments), between 50 MHz and 600 MHz. The error signal was fed to a PI servo controller (LB1005-S, New Focus) which acts on the driving current of DFB-QCL2. Optionally, f_{beat} was down-mixed with a frequency f_{down} prior to being mixed with f_{sweep} .

Synchronously with the sweep, the beam of the DFB is detected using PD3 after passing through a gas cell and the DC transmission is recorded.

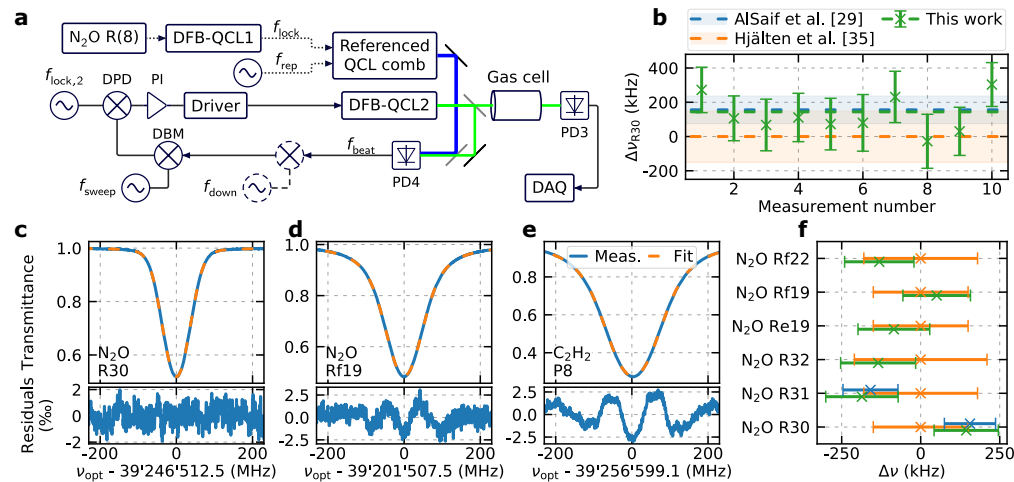


Fig. 3. Assessment of the absolute frequency accuracy and comb-calibrated spectroscopy. (a) Setup. DAQ: data acquisition unit. (b) Comparison of 10 measurements of the frequency of transition R(30) against literature references with 1 σ error bars. The uncertainty of the literature data is represented with the background color. (c-e) Transmittance, fit and residuals of 3 selected transitions. (f) Comparison of the obtained transition frequencies with literature values. The color code follows from (b).

This setup allowed us to perform frequency-calibrated spectroscopic measurements of molecular transitions by sweeping the offset between the stabilized QCL-OFC and DFB-QCL2 in any 550 MHz range between 100 MHz and 1.5 GHz while maintaining their phase lock. The 1.5-GHz bandwidth for the offsets between the DFBs and the comb gives, assuming a fixed transition frequency for DFB-QCL1, a 6-GHz coverage for DFB-QCL2, which represents two thirds of the free spectral range of the comb used in this experiment. Full access could be obtained by changing the locking transition of DFB-QCL1.

Assessment of the frequency accuracy

As a first step, we measured the transition R(30) of N_2O at 1.5 mbar through a 1-cm length gas cell [Fig. 3(c)]. The referencing of the comb to a known transition and the knowledge of all the RF frequencies determines the absolute frequency of DFB-QCL2 within the ambiguity given by the repetition rate of the comb. This ambiguity is lifted by the approximate knowledge of the transition of interest. The sweep over 550 MHz takes 20 s. We fit the frequency-calibrated transmission using a Voigt profile which gives us the center frequency of the transition.

To assess the accuracy of our setup, we performed 10 sets of measurement of the transition R(30). Each set of measurement involved the following steps: (i) scanning DFB-QCL1 10 times over transition R(8) in an open loop to determine Δ_f , as described in section 2, (ii) locking of DFB-QCL1 to transition R(8), (iii) locking of the comb to DFB-QCL1, (iv) sweeping DFB-QCL2 over the resonance 10 times in each direction (20 sweeps in total). Each set of measurement took about 12 minutes (6.6 minutes of actual measurement), and resulted in an absolute frequency value for the transition R(30), which is shown and compared with the measurements of AlSaif *et al.* [29] and Hjalten *et al.* [35] in Fig. 3(b). The 10 sets were performed in the span of a week. Most data points agree with the references and to each other within 1σ uncertainty, showing that the estimated uncertainties are coherent and unaccounted-for biases are within the uncertainties.

The uncertainty budget for one measurement set is given in Table 1. Through the 10 scans over transition R(8), we obtain 10 measurements of Δ_f with a standard deviation ranging between 236 kHz and 392 kHz, such that the type A uncertainty of the mean is between 78 kHz and 131 kHz (average 103 kHz). We considered a systematic bias of Δ_f of (-83 ± 22) kHz due to the finite scanning speed, measured by scanning in the opposite direction.

Table 1. Uncertainty Budget For 1 Measurement Set

	Type A Uncertainty (kHz)	Type B Uncertainty (kHz)
Offset Δ_f of the locking point from the transition center (10 scans)	78-131	
Δ_f bias uncertainty		22
Fit uncertainty (20 sweeps)	6-10	
Stability of the comb	20	
Pressure shift		60
R8 transition frequency [29]		72
Total uncertainty (1 σ)	128-165	

The 20 sweeps of DFB-QCL2 and their fits show a standard deviation of the center frequency of the R(30) transition between 28 kHz and 44 kHz, such that the standard deviation of the mean is between 6 kHz and 10 kHz (average 8 kHz). The frequency stability of DFB-QCL1 over the measurement time of 15 minutes is 20 kHz.

We also estimated a 60-kHz uncertainty due to pressure shift, corresponding to 2 mbar pressure uncertainty on the gas cells. Indeed, the sealed commercial gas cells contained an undesired high ratio of water vapor, which complicated the task of determining the exact pressure and concentrations of the cells. The R(8) transition is known within 72 kHz [29]. We obtain an uncertainty ranging from 128 kHz to 165 kHz (average 145 kHz) for each set of measurement of the R(30) transition. The uncertainty is reduced to 102 kHz (fractional accuracy of $3 \cdot 10^{-9}$) on the mean of the 10 measurements (using inverse variance weighting). This cannot be significantly improved by repeated measurements since the overall uncertainty is rapidly dominated by the type B uncertainties.

Spectroscopic measurements

As the performance of the frequency-calibrated spectrometer has been assessed, we used it to determine the absolute frequency of other transitions. We studied the additional transitions R(31) and R(32) of the ν_1 fundamental band of N_2O using the same gas cell. Moreover, we studied transitions Re(19), Rf(19), Re(22), and Rf(22) of the $(11^1_0) \leftarrow (01^1_0)$ hot band of N_2O using a 10-cm gas cell filled with 15% N_2O at 9 mbar. Unfortunately, the presence of a strong transition near Re(22) did not allow us to make a correct fit of the latter. Finally, we also measured transition P(8) of C_2H_2 through a 8-cm gas cell filled with 12% C_2H_2 at 8 mbar, for which the best available uncertainty is between 3 MHz and 30 MHz [61]. For each transition, we acquired 3 sets of measurements [2 for transition Rf(22)]. For each set, between 10 and 32 scans of DFB-QCL1 and between 10 and 20 sweeps of DFB-QCL2 were acquired. The total uncertainty remains in the same order of magnitude. The final transition frequency and its uncertainty is determined using inverse variance weighting.

We show typical transmission spectra (acquired in one 20-s sweep) and their fit in Fig. 3(c-e) for the transitions R(30) and Rf(19) of N_2O and P(8) of C_2H_2 . The obtained transition frequencies are given in Table 2. Moreover, Fig. 3(f) shows the comparison of the obtained N_2O transition frequencies against the available references. All results agree with the literature within the specified uncertainties.

Table 2. Spectroscopic Data

Transition	Measured Line Center (cm ⁻¹)	Literature (cm ⁻¹)
N ₂ O R(30)	1309.122743(3)	1309.1227432(27) [29], 1309.122738(5) [35]
N ₂ O R(31)	1309.846770(4)	1309.8467707(29) [29], 1309.846776(6) [35]
N ₂ O R(32)	1310.567203(4)	1310.567207(7) [35]
N ₂ O Re(19)	1307.540325(4)	1307.540328(5) [35]
N ₂ O Rf(19)	1307.621542(4)	1307.621540(5) [35]
N ₂ O Rf(22)	1309.928550(4)	1309.928554(6) [35]
C ₂ H ₂ P(8)	1309.459305(4)	1309.4592(10) [61]

5. Discussion and conclusion

For the first time, to the best of our knowledge, we have fully stabilized a MIR QCL-OFC to a molecular transition and characterized it. All comb lines are known with $3 \cdot 10^{-9}$ relative frequency accuracy, and their relative stability is $1.5 \cdot 10^{-10}$ at 100-s integration time and $5 \cdot 10^{-10}$ at 1000-s integration time. Moreover, we performed comb-referenced laser absorption spectroscopy. This work thus demonstrates the suitability of MIR QCL-OFCs to be used as frequency references.

The limits in frequency stability and accuracy do not originate from the comb itself, but from the laser locked to the molecular transition and from the pressure shift. The actual limit of the QCL-OFC remains to be assessed, but stabilities as good as 1 Hz at 1-s integration time can be expected from the in-loop stability of the locked beat signals. Locking of the QCL-OFC to state-of-the-art MIR sub-Doppler references [55–59] with stabilities down to the sub-Hz level could open paths for MIR metrological studies. However, the accuracies demonstrated in this work are already comparable to other works requiring nonlinear frequency conversion [29,35] and are largely sufficient for room-temperature Doppler-limited spectroscopy.

The large free spectral range of 10 GHz of the QCL-OFC is practical for closed-loop comb-assisted spectroscopy over hundreds of MHz, as the problem of the heterodyne beat reaching near zero frequency and folding is avoided [21,34]. However, the available detectors can provide sufficient SNR for phase-locking only up to 1.5-GHz offsets, such that accessing the full optical spectrum requires changing the transition frequency of the locked laser. A smaller free spectral range on the order of 2-5 GHz is preferred in this regard. This issue also needs to be solved for referencing a swept dual comb spectrometer [62], where the beat between the comb and the locked laser will span half of the free spectral range.

Lastly, the bandwidth of the spectroscopy was limited by DFB-QCL2 to a few wavenumbers. The use of an external cavity QCL and state-of-the-art QCL-OFCs [60] would allow to reach bandwidths of 70 cm⁻¹, competing with the existing techniques based on nonlinear frequency conversion [29,35]. In the near-future, broadening of the comb bandwidth, frequency referencing in a swept dual comb spectrometer, and self-referencing are three advances that will make QCL-OFCs more performant and attractive for MIR spectroscopy.

Funding. Swiss Space Office (MdP COSMICS); Schweizerischer Nationalfonds zur Förderung der Wissenschaftlichen Forschung (200020_178864, 40B2-1_176584); Horizon 2020 Framework Programme (871529).

Acknowledgement. We thank Alpes Lasers for providing the two DFB-QCLs used in this experiment. We acknowledge insightful discussions with Alexandre Parriaux.

Disclosures. The authors declare no conflicts of interest.

Data availability. Data underlying the results presented in this paper are available EUDAT B2SHARE repository: b2share (2021), Ref. [63].

References

1. A. Schliesser, N. Picqué, and T. W. Hänsch, “Mid-infrared frequency combs,” *Nat. Photonics* **6**(7), 440–449 (2012).

2. J. Haas and B. Mizaikoff, "Advances in Mid-Infrared Spectroscopy for Chemical Analysis," *Annu. Rev. Anal. Chem.* **9**(1), 45–68 (2016).
3. C. J. Breshike, C. A. Kendziora, R. Furstenberg, T. J. Huffman, V. Nguyen, N. Budack, Y. Yoon, and R. A. McGill, "Hyperspectral imaging using active infrared backscatter spectroscopy for detection of trace explosives," *Opt. Eng.* **59**(09), 1 (2020).
4. N. M. Ralbovsky and I. K. Lednev, "Vibrational Spectroscopy for Detection of Diabetes: A Review," *Appl. Spectrosc.* **75**(8), 929–946 (2021).
5. M. De Marchi, V. Toffanin, M. Cassandro, and M. Penasa, "Invited review: Mid-infrared spectroscopy as phenotyping tool for milk traits," *J. Dairy Sci.* **97**(3), 1171–1186 (2014).
6. ÁI López-Lorente and B. Mizaikoff, "Mid-infrared spectroscopy for protein analysis: potential and challenges," *Anal. Bioanal. Chem.* **408**(11), 2875–2889 (2016).
7. V. Villanueva-López, L. C. Pacheco-Londoño, R. Villarreal-González, J. R. Castro-Suarez, A. Román-Ospino, W. Ortiz-Rivera, N. J. Galán-Freyte, and S. P. Hernandez-Rivera, "API Content and Blend Uniformity Using Quantum Cascade Laser Spectroscopy Coupled with Multivariate Analysis," *Pharmaceutics* **13**(7), 985 (2021).
8. G. Ycas, F. R. Giorgetta, J. T. Friedlein, D. Herman, K. C. Cossel, E. Baumann, N. R. Newbury, and I. Coddington, "Compact mid-infrared dual-comb spectrometer for outdoor spectroscopy," *Opt. Express* **28**(10), 14740 (2020).
9. T. Udem, R. Holzwarth, and T. W. Hänsch, "Optical frequency metrology," *Nature* **416**(6877), 233–237 (2002).
10. B. Argence, B. Chanteau, O. Lopez, D. Nicolodi, M. Abgrall, C. Chardonnet, C. Daussy, B. Darquié, Y. Le Coq, and A. Amy-Klein, "Quantum cascade laser frequency stabilization at the sub-Hz level," *Nat. Photonics* **9**(7), 456–460 (2015).
11. N. Picqué and T. W. Hänsch, "Frequency comb spectroscopy," *Nat. Photonics* **13**(3), 146–157 (2019).
12. Z. Zhang, T. Gardiner, and D. T. Reid, "Mid-infrared dual-comb spectroscopy with an optical parametric oscillator," *Opt. Lett.* **38**(16), 3148–3150 (2013).
13. I. Coddington, N. Newbury, and W. Swann, "Dual-comb spectroscopy," *Optica* **3**(4), 414–426 (2016).
14. G. Ycas, F. R. Giorgetta, E. Baumann, I. Coddington, D. Herman, S. A. Diddams, and N. R. Newbury, "High-coherence mid-infrared dual-comb spectroscopy spanning 2.6 to 5.2 μm ," *Nat. Photonics* **12**(4), 202–208 (2018).
15. A. V. Muraviev, V. O. Smolski, Z. E. Loparo, and K. L. Vodopyanov, "Massively parallel sensing of trace molecules and their isotopologues with broadband subharmonic mid-infrared frequency combs," *Nat. Photonics* **12**(4), 209–214 (2018).
16. H. Timmers, A. Kowligy, A. Lind, F. C. Cruz, N. Nader, M. Silfies, G. Ycas, T. K. Allison, P. G. Schunemann, S. B. Papp, and S. A. Diddams, "Molecular fingerprinting with bright, broadband infrared frequency combs," *Optica* **5**(6), 727–732 (2018).
17. J. Mandon, G. Guelachvili, and N. Picqué, "Fourier transform spectroscopy with a laser frequency comb," *Nat. Photonics* **3**(2), 99–102 (2009).
18. F. Adler, P. Masłowski, A. Foltynowicz, K. C. Cossel, T. C. Briles, I. Hartl, and J. Ye, "Mid-infrared Fourier transform spectroscopy with a broadband frequency comb," *Opt. Express* **18**(21), 21861–21872 (2010).
19. P. Del'Haye, O. Arcizet, M. L. Gorodetsky, R. Holzwarth, and T. J. Kippenberg, "Frequency comb assisted diode laser spectroscopy for measurement of microcavity dispersion," *Nat. Photonics* **3**(9), 529–533 (2009).
20. M. Lamperti, B. AlSaif, D. Gatti, M. Fermann, P. Laporta, A. Farooq, and M. Marangoni, "Absolute spectroscopy near 7.8 μm with a comb-locked extended-cavity quantum-cascade-laser," *Sci. Rep.* **8**(1), 1292 (2018).
21. R. Gotti, T. Puppe, Y. Mayzlin, J. Robinson-Tait, S. Wójciewicz, D. Gatti, B. Alsaif, M. Lamperti, P. Laporta, F. Rohde, R. Wilk, P. Leisching, W. G. Kaenders, and M. Marangoni, "Comb-locked frequency-swept synthesizer for high precision broadband spectroscopy," *Sci. Rep.* **10**(1), 2523 (2020).
22. H. Guo, W. Weng, J. Liu, F. Yang, W. Hänsel, C. S. Brès, L. Thévenaz, R. Holzwarth, T. J. Kippenberg, and T. J. Kippenberg, "Nanophotonic supercontinuum-based mid-infrared dual-comb spectroscopy," *Optica* **7**(9), 1181–1188 (2020).
23. E. Baumann, F. R. Giorgetta, W. C. Swann, A. M. Zolot, I. Coddington, and N. R. Newbury, "Spectroscopy of the methane ν_3 band with an accurate midinfrared coherent dual-comb spectrometer," *Phys. Rev. A* **84**(6), 062513 (2011).
24. E. Baumann, E. V. Hoenig, E. F. Perez, G. M. Colacion, F. R. Giorgetta, K. C. Cossel, G. Ycas, D. R. Carlson, D. D. Hickstein, K. Srinivasan, S. B. Papp, N. R. Newbury, and I. Coddington, "Dual-comb spectroscopy with tailored spectral broadening in Si_3N_4 nanophotonics," *Opt. Express* **27**(8), 11869 (2019).
25. A. Amy-Klein, A. Goncharov, C. Daussy, C. Grain, O. Lopez, G. Santarelli, and C. Chardonnet, "Absolute frequency measurement in the 28-THz spectral region with a femtosecond laser comb and a long-distance optical link to a primary standard," *Appl. Phys. B* **78**(1), 25–30 (2004).
26. A. Gambetta, N. Coluccelli, M. Cassinerio, T. T. Fernandez, D. Gatti, A. Castrillo, A. Ceausu-Velcescu, E. Fasci, L. Gianfrani, L. Santamaria, V. Di Sarno, P. Maddaloni, P. De Natale, P. Laporta, and G. Galzerano, "Frequency-comb-assisted precision laser spectroscopy of CHF_3 around 8.6 μm ," *J. Chem. Phys.* **143**(23), 234202 (2015).
27. A. Gambetta, M. Cassinerio, N. Coluccelli, E. Fasci, A. Castrillo, L. Gianfrani, D. Gatti, M. Marangoni, P. Laporta, and G. Galzerano, "Direct phase-locking of a 8.6- μm quantum cascade laser to a mid-IR optical frequency comb: application to precision spectroscopy of N_2O ," *Opt. Lett.* **40**(3), 304–307 (2015).

28. A. Gambetta, E. Vicentini, Y. Wang, N. Coluccelli, E. Fasci, L. Gianfrani, A. Castrillo, V. D. Sarno, L. Santamaria, P. Maddaloni, P. D. Natale, P. Laporta, and G. Galzerano, "Absolute frequency measurements of CHF_3 Doppler-free ro-vibrational transitions at 8.6 μm ," *Opt. Lett.* **42**(10), 1911–1914 (2017).
29. B. AlSaif, M. Lamperti, D. Gatti, P. Laporta, M. Fermann, A. Farooq, O. Lyulin, A. Campargue, and M. Marangoni, "High accuracy line positions of the ν_1 fundamental band of $^{14}\text{N}_2^{16}\text{O}$," *J. Quant. Spectrosc. Radiat. Transfer* **211**, 172–178 (2018).
30. A. Gambetta, E. Vicentini, N. Coluccelli, Y. Wang, T. T. Fernandez, P. Maddaloni, P. De Natale, A. Castrillo, L. Gianfrani, P. Laporta, and G. Galzerano, "Versatile mid-infrared frequency-comb referenced sub-Doppler spectrometer," *APL Photonics* **3**(4), 046103 (2018).
31. B. AlSaif, D. Gatti, M. Lamperti, P. Laporta, A. Farooq, and M. Marangoni, "Comb-calibrated sub-Doppler spectroscopy with an external-cavity quantum cascade laser at 7.7 μm ," *Opt. Express* **27**(17), 23785–23790 (2019).
32. R. Santagata, D. B. A. Tran, B. Argence, O. Lopez, S. K. Tokunaga, F. Wiotte, H. Mouhamad, A. Goncharov, M. Abgrall, Y. L. Coq, H. Alvarez-Martinez, R. L. Targat, W. K. Lee, D. Xu, P.-E. Pottie, B. Darquié, and A. Amy-Klein, "High-precision methanol spectroscopy with a widely tunable SI-traceable frequency-comb-based mid-infrared QCL," *Optica* **6**(4), 411–423 (2019).
33. P. B. Changala, M. L. Weichman, K. F. Lee, M. E. Fermann, and J. Ye, "Rovibrational quantum state resolution of the C 60 fullerene," *Science* **363**(6422), 49–54 (2019).
34. M. Lamperti, R. Gotti, D. Gatti, M. K. Shakfa, E. Cané, F. Tamassia, P. Schunemann, P. Laporta, A. Farooq, and M. Marangoni, "Optical frequency metrology in the bending modes region," *Commun. Phys.* **3**(1), 175 (2020).
35. A. Hjältén, M. Germann, K. Krzempek, A. Hudzikowski, A. Gluszek, D. Tomaszewska, G. Soboń, and A. Foltynowicz, "Optical frequency comb Fourier transform spectroscopy of $^{14}\text{N}_2^{16}\text{O}$ at 7.8 μm ," *J. Quant. Spectrosc. Radiat. Transfer* **271**, 107734 (2021).
36. A. Hugi, G. Villares, S. Blaser, H. C. Liu, and J. Faist, "Mid-infrared frequency comb based on a quantum cascade laser," *Nature* **492**(7428), 229–233 (2012).
37. J. Faist, G. Villares, G. Scalari, M. Rösch, C. Bonzon, A. Hugi, and M. Beck, "Quantum Cascade Laser Frequency Combs," *Nanophotonics* **5**(2), 272–291 (2016).
38. E. Lins, S. Read, B. Unni, S. M. Rosendahl, and I. J. Burgess, "Microsecond Resolved Infrared Spectroelectrochemistry Using Dual Frequency Comb IR Lasers," *Anal. Chem.* **92**(9), 6241–6244 (2020).
39. J. L. Klocke, M. Mangold, P. Allmendinger, A. Hugi, M. Geiser, P. Jouy, J. Faist, and T. Kottke, "Single-Shot Sub-microsecond Mid-infrared Spectroscopy on Protein Reactions with Quantum Cascade Laser Frequency Combs," *Anal. Chem.* **90**(17), 10494–10500 (2018).
40. G. Villares, A. Hugi, S. Blaser, and J. Faist, "Dual-comb spectroscopy based on quantum-cascade-laser frequency combs," *Nat. Commun.* **5**(1), 5192 (2014).
41. F. Cappelli, G. Campo, I. Galli, G. Giusfredi, S. Bartalini, D. Mazzotti, P. Cancio, S. Borri, B. Hinkov, J. Faist, and P. De Natale, "Frequency stability characterization of a quantum cascade laser frequency comb," *Laser Photonics Rev.* **10**(4), 623–630 (2016).
42. F. Cappelli, L. Consolino, G. Campo, I. Galli, D. Mazzotti, A. Campa, M. Siciliani de Cumis, P. Cancio Pastor, R. Eramo, M. Rösch, M. Beck, G. Scalari, J. Faist, P. De Natale, and S. Bartalini, "Retrieval of phase relation and emission profile of quantum cascade laser frequency combs," *Nat. Photonics* **13**(8), 562–568 (2019).
43. K. Komagata, A. Shehzad, G. Terrasanta, P. Brochard, R. Matthey, M. Gianella, P. Jouy, F. Kapsalidis, M. Shahmohammadi, M. Beck, V. J. Wittwer, J. Faist, L. Emmenegger, T. Südmeyer, A. Hugi, and S. Schilt, "Coherently-averaged dual comb spectrometer at 7.7 μm with master and follower quantum cascade lasers," *Opt. Express* **29**(12), 19126–19139 (2021).
44. J. Hillbrand, A. M. Andrews, H. Detz, G. Strasser, and B. Schwarz, "Coherent injection locking of quantum cascade laser frequency combs," *Nat. Photonics* **13**(2), 101–104 (2019).
45. M. R. St-Jean, M. I. Amanti, A. Bernard, A. Calvar, A. Bismuto, E. Gini, M. Beck, J. Faist, H. C. Liu, and C. Sirtori, "Injection locking of mid-infrared quantum cascade laser at 14 GHz, by direct microwave modulation," *Laser Photonics Rev.* **8**(3), 443–449 (2014).
46. F. Kapsalidis, B. Schneider, M. Singleton, M. Bertrand, E. Gini, M. Beck, and J. Faist, "Mid-infrared quantum cascade laser frequency combs with a microstrip-like line waveguide geometry," *Appl. Phys. Lett.* **118**(7), 071101 (2021).
47. M. Singleton, P. Jouy, M. Beck, and J. Faist, "Evidence of linear chirp in mid-infrared quantum cascade lasers," *Optica* **5**(8), 948–953 (2018).
48. L. Consolino, M. Nafa, F. Cappelli, K. Garrasi, F. P. Mezzapesa, L. Li, A. G. Davies, E. H. Linfield, M. S. Vitiello, P. De Natale, and S. Bartalini, "Fully phase-stabilized quantum cascade laser frequency comb," *Nat. Commun.* **10**(1), 2938 (2019).
49. L. Consolino, M. Nafa, M. De Regis, F. Cappelli, K. Garrasi, F. P. Mezzapesa, L. Li, A. G. Davies, E. H. Linfield, M. S. Vitiello, S. Bartalini, and P. De Natale, "Quantum cascade laser based hybrid dual comb spectrometer," *Commun. Phys.* **3**(1), 69 (2020).
50. J. Westberg, L. A. Sterczewski, and G. Wysocki, "Mid-infrared multiheterodyne spectroscopy with phase-locked quantum cascade lasers," *Appl. Phys. Lett.* **110**(14), 141108 (2017).

51. H. R. Telle, G. Steinmeyer, A. E. Dunlop, J. Stenger, D. H. Sutter, and U. Keller, "Carrier-envelope offset phase control: A novel concept for absolute optical frequency measurement and ultrashort pulse generation," *Appl. Phys. B* **69**(4), 327–332 (1999).
52. J. Hillbrand, N. Opačák, M. Piccardo, H. Schneider, G. Strasser, F. Capasso, and B. Schwarz, "Mode-locked short pulses from an 8 μm wavelength semiconductor laser," *Nat. Commun.* **11**(1), 5788 (2020).
53. P. Täschler, M. Bertrand, B. Schneider, M. Singleton, P. Jouy, F. Kapsalidis, M. Beck, and J. Faist, "Femtosecond pulses from a mid-infrared quantum cascade laser," *Nat. Photonics* **15**(12), 919–924 (2021).
54. C. C. Teng, J. Westberg, and G. Wysocki, "Frequency Stabilization of a Quantum Cascade Dual-Comb Spectrometer to a Molecular Transition," in *Conference on Lasers and Electro-Optics (CLEO)* (2020), paper SF2G.3.
55. O. Acef, "Metrological properties of CO₂O₄ optical frequency standard," *Opt. Commun.* **134**(1-6), 479–486 (1997).
56. V. Bernard, C. Daussy, G. Nogues, L. Constantin, P. E. Durand, A. Amy-Klein, A. V. Lerberghe, and C. Chardonnet, "CO₂ laser stabilization to 0.1-Hz level using external electrooptic modulation," *IEEE J. Quantum Electron.* **33**(8), 1282–1287 (1997).
57. F. Cappelli, I. Galli, S. Borri, G. Giusfredi, P. Cancio, D. Mazzotti, A. Montori, N. Akikusa, M. Yamanishi, S. Bartalini, and P. D. Natale, "Subkilohertz linewidth room-temperature mid-infrared quantum cascade laser using a molecular sub-Doppler reference," *Opt. Lett.* **37**(23), 4811–4813 (2012).
58. P. L. T. Sow, S. Mejri, S. K. Tokunaga, O. Lopez, A. Goncharov, B. Argenç, C. Chardonnet, A. Amy-Klein, C. Daussy, and B. Darquié, "A widely tunable 10- μm quantum cascade laser phase-locked to a state-of-the-art mid-infrared reference for precision molecular spectroscopy," *Appl. Phys. Lett.* **104**(26), 264101 (2014).
59. E. Vicentini, A. Gambetta, N. Coluccelli, V. Di Sarno, P. Maddaloni, P. De Natale, A. Castrillo, L. Gianfrani, P. Laporta, and G. Galzerano, "Absolute frequency stabilization of a QCL at 8.6 μm by modulation transfer spectroscopy," *Opt. Lett.* **45**(17), 4948 (2020).
60. P. Jouy, J. M. Wolf, Y. Bidaux, P. Allmendinger, M. Mangold, M. Beck, and J. Faist, "Dual comb operation of $\lambda \sim 8.2$ μm quantum cascade laser frequency comb with 1 W optical power," *Appl. Phys. Lett.* **111**(14), 141102 (2017).
61. I. E. Gordon, L. S. Rothman, C. Hill, R. V. Kochanov, Y. Tan, P. F. Bernath, M. Birk, V. Boudon, A. Campargue, K. V. Chance, B. J. Drouin, J.-M. Flaud, R. R. Gamache, J. T. Hodges, D. Jacquemart, V. I. Perevalov, A. Perrin, K. P. Shine, M.-A. H. Smith, J. Tennyson, G. C. Toon, H. Tran, V. G. Tyuterev, A. Barbe, A. G. Császár, V. M. Devi, T. Furtenbacher, J. J. Harrison, J.-M. Hartmann, A. Jolly, T. J. Johnson, T. Karman, I. Kleiner, A. A. Kyuberis, J. Loos, O. M. Lyulin, S. T. Massie, S. N. Mikhailenko, N. Moazzen-Ahmadi, H. S. P. Müller, O. V. Naumenko, A. V. Nikitin, O. L. Polyansky, M. Rey, M. Rotger, S. W. Sharpe, K. Sung, E. Starikova, S. A. Tashkun, J. V. Auwera, G. Wagner, J. Wilzewski, P. Wcisło, S. Yu, and E. J. Zak, "The HITRAN2016 molecular spectroscopic database," *J. Quant. Spectrosc. Radiat. Transfer* **203**, 3–69 (2017).
62. M. Gianella, A. Nataraj, B. Tuzson, P. Jouy, F. Kapsalidis, M. Beck, M. Mangold, A. Hugi, J. Faist, and L. Emmenegger, "High-resolution and gapless dual comb spectroscopy with current-tuned quantum cascade lasers," *Opt. Express* **28**(5), 6197–6208 (2020).
63. K. Komagata, M. Gianella, P. Jouy, F. Kapsalidis, M. Shahmohammadi, M. Beck, R. Matthey, V. J. Wittwer, A. Hugi, J. Faist, L. Emmenegger, T. Südmeyer, and S. Schilt EUDAT B2SHARE Repository", b2share, (2021). <http://doi.org/10.23728/b2share.b84f40e2619846298a125f831a737f4e>